

# ATLAS ITk strip sensor quality assurance tests and results of ATLAS18 pre-production sensors

S. HIROSE<sup>1</sup>, P. ALLPORT<sup>2</sup>, E. BACH<sup>3</sup>, M.J. BASSO<sup>4</sup>, A. BHARDWAJ<sup>4</sup>, A. CHISHOLM<sup>2</sup>, V. CINDRO<sup>5</sup>, B. CIUNGU<sup>4</sup>, B. CRICK<sup>4</sup>, J. FERNANDEZ-TEJERO<sup>6,7</sup>, C. FLETA<sup>3</sup>, W. GOERGE<sup>2</sup>, L. GONELLA<sup>2</sup>, K. HARA<sup>1</sup>, A. HUNTER<sup>2</sup>, T. ISHII<sup>1</sup>, T. KNIGHT<sup>4</sup>, I. KOPSALIS<sup>2</sup>, J. KROLL<sup>8</sup>, J. KVASNICKA<sup>8</sup>, V. LATONOVA<sup>8</sup>, J. LOMAS<sup>2</sup>, I. MANDIĆ<sup>5</sup>, M. MIKESTIKOVA<sup>8</sup>, K. NAKAMURA<sup>9</sup>, R.S. ORR<sup>4</sup>, K. SAITO<sup>1</sup>, M. ULLÁN<sup>3</sup>, Y. UNNO<sup>9</sup>

<sup>1</sup>*Institute of Pure and Applied Sciences, University of Tsukuba, 1-1-1 Tennodai, Tsukuba, Ibaraki 305-8571, Japan*

<sup>2</sup>*School of Physics and Astronomy, University of Birmingham, Birmingham B152TT, United Kingdom*

<sup>3</sup>*Instituto de Microelectronica de Barcelona (IMB-CNM, CSIC), Campus UAB-Bellaterra, 08193 Barcelona, Spain*

<sup>4</sup>*Department of Physics, University of Toronto, 60 Saint George St., Toronto, Ontario M5S1A7, Canada*

<sup>5</sup>*Experimental Particle Physics Department, Jožef Stefan Institute, Jamova 39, SI-1000 Ljubljana, Slovenia*

<sup>6</sup>*Department of Physics, Simon Fraser University, 8888 University Drive, Burnaby, B.C. V5A 1S6, Canada*

<sup>7</sup>*TRIUMF, 4004 Wesbrook Mall, Vancouver, B.C. V6T 2A3, Canada*

<sup>8</sup>*Academy of Sciences of the Czech Republic, Institute of Physics, Na Slovance 2, 18221 Prague 8, Czech Republic*

<sup>9</sup>*Institute of Particle and Nuclear Study, High Energy Accelerator Research Organization (KEK), 1-1 Oho, Tsukuba, Ibaraki 305-0801, Japan*

*E-mail: shhirose@hep.px.tsukuba.ac.jp*

(Received January 13, 2023)

Towards the high luminosity (HL) operation of the Large Hadron Collider (LHC), the inner tracking system of the ATLAS detector will be replaced by a fully silicon-based inner tracker (ITk). Its outer region consists of 17,888  $n^+$ -in- $p$  silicon strip sensors. In order to confirm key properties of the production sensors as well as to establish a solid workflow of quality inspection and monitoring of the various sensor properties, about 5% of the total strip sensors were produced in 2020 as a pre-production run. As a quality assurance (QA) program, irradiation of dedicated QA test pieces was periodically performed. The fluences of proton, neutron and  $\gamma$ -ray irradiations were up to  $1.6 \times 10^{15}$  1- $\text{MeV}$  neutrons/ $\text{cm}^2$  and 0.66 MGy, which are equivalent to the maximum expected radiation fluences at the HL-LHC operation with a safety factor of 1.5. Results from 154 QA test pieces demonstrated high quality of the strip sensors through the pre-production. Detailed understanding of post-irradiated strip sensors was acquired, and the procedures of irradiation and post-irradiation QA testing were fully established. Consequently, the 3.8-year project of the strip sensor production for the ATLAS ITk detector was initiated in July 2021.

**KEYWORDS:** HL-LHC, ATLAS, silicon detector, strip sensor, radiation damage



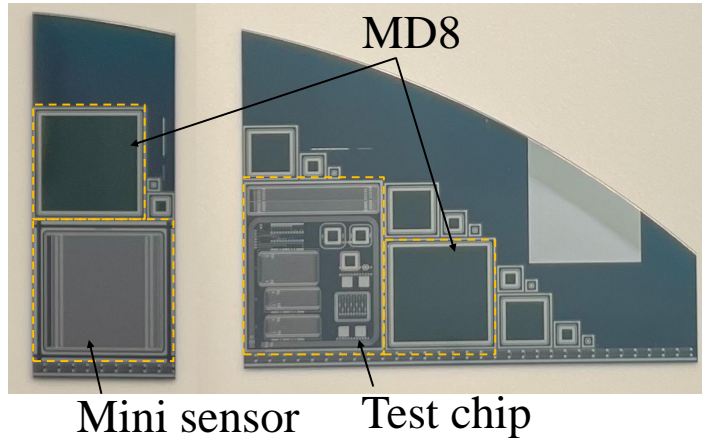


**Fig. 1.** Photos of the QA test pieces. The left structure holds a mini sensor and an MD8 while the right one a test chip and an MD8.

## 1. Introduction

The Large Hadron Collider (LHC) will start its high-luminosity (HL) operation in 2029, aiming at an instantaneous luminosity of  $7.5 \times 10^{34} \text{ cm}^{-2}\text{s}^{-1}$  and an integrated luminosity of  $4000 \text{ fb}^{-1}$ , after major upgrades on the accelerator components following the ongoing Run-3 operation (2022–2025). The ATLAS detector will be also largely upgraded to cope with about three times higher pile-up than the current experimental conditions as well as to improve its performance. One of the key upgrades is the replacement of the current inner tracking system by the inner tracker (ITk). The ITk has a cylindrical structure with a  $\sim 1 \text{ m}$  radius and a  $\sim 6 \text{ m}$  long. The inner region is composed of silicon pixel sensors [1, 2] while the outer region of silicon strip sensors [3].

The strip part (ITk Strips) consists of four layers on the barrel and six disks in both endcaps. The entire area of  $165 \text{ m}^2$  is covered by 17,888 silicon strip modules, where one module has one strip sensor and several readout ASICs; details of the ITk Strip module can be found in Ref. [3]. For the barrel, a  $320\text{-}\mu\text{m}$ -thick  $n^+$ -on- $p$  strip sensor with a dimension of  $9.8 \times 9.8 \text{ cm}^2$  is employed. The sensor has 1282 strips segmented by two or four sections. For the endcaps, the sensor has the similar properties but a different shape depending on the region.

Following successful developments, the ATLAS18 strip sensor was designed as the production version for the ITk Strips [4]. During the mass production of the strip sensors, important properties will be inspected in order to assure their quality, and to reject sensors with unsatisfactory performance. These inspections are divided into two categories; quality control (QC) is a series of inspections on the fundamental sensor properties, such as a shape, a leakage current and its stability, etc., of the main sensors so that possible defects can be identified, while quality assurance (QA) aims at monitoring of radiation tolerance using dedicated QA test pieces [5] on a sampling basis. Decision to accept or reject the sensors will be made based on well-defined criteria for both QC and QA.

In advance to the mass production for 20,800 strip sensors (including 15% extra sensors to account for assembly yields of the modules, barrel staves and endcap petals), 1040 wafers were pre-produced in 2020, equivalent to 5% of the production number of wafers. Together with additional 60 prototype wafers, 1101 wafers were used to understand performance of the final-version strip sensors in detail, as well as to establish QC and QA procedures. For pre-production QA, 154 QA test pieces were irradiated. Those QA test pieces, shown in Fig. 1, include a  $10 \times 10 \text{ mm}^2$  strip sensor (mini sensor), a simple  $8 \times 8 \text{ mm}^2$  diode structure (MD8) and a small chip with various structures dedicated to the measurement of specific wafer properties (test chip). These QA test pieces are fabricated on the

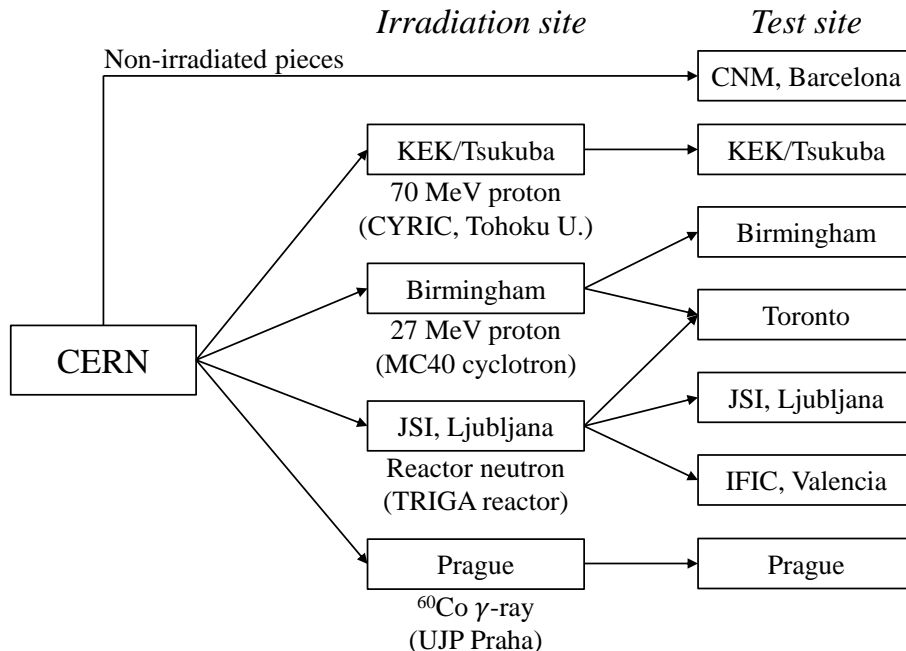


**Fig. 2.** Flow chart of the strip sensor QA test pieces for the pre-production QA.

same wafer as the main sensor. Therefore evaluation of basic technological properties of the wafer is possible without irradiating to the large-area main sensor. Typically, each type of the QA pieces are chosen from one batch, which typically contains  $\sim 40$  wafers, and irradiated by protons, neutrons or  $\gamma$ -rays.

In this paper, the QA criteria established during the pre-production as well as results from the pre-production QA are summarised, with updates from the previous publication [6].

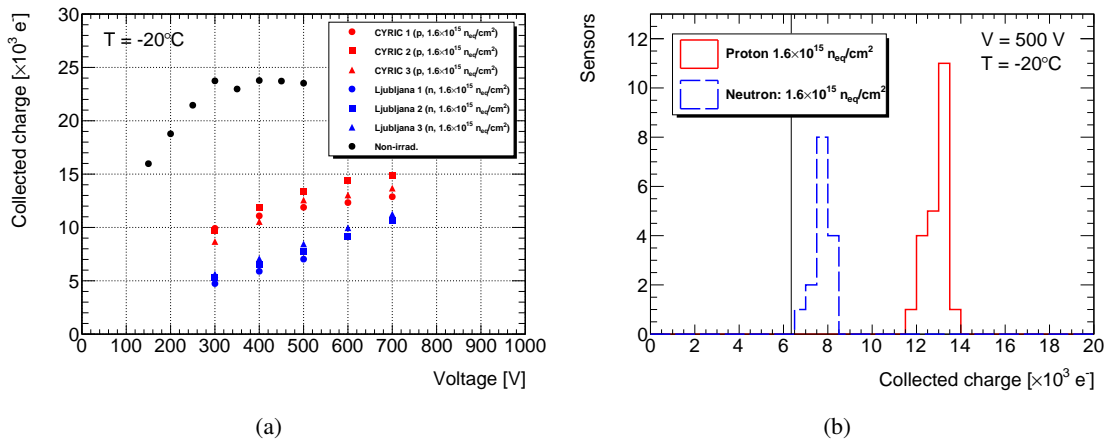
## 2. Procedure for strip sensor quality assurance

Figure 2 shows a flow chart of the strip sensor QA during the pre-production. All QA pieces were first delivered to CERN, and then distributed to each irradiation site. High Energy Accelerator Research Organization (KEK, Japan), University of Tsukuba (Japan) and University of Birmingham (UK) were responsible for proton irradiation. The Japan cluster performed irradiation using a 70 MeV proton beam provided by the Cyclotron and Radioisotope Center (CYRIC) of Tohoku University (Japan) [7], and tested the irradiated QA test pieces at KEK. The Birmingham group irradiated 27 MeV protons from the MC40 cyclotron [8]. Half of the irradiated QA test pieces were measured at Birmingham, and the rest were sent to University of Toronto (Canada). The total ionisation dose (TID) per  $10^{15}$  1-MeV neutrons( $n_{eq}$ )/cm $^2$  were expected to be 0.77 MGy and 1.44 MGy at CYRIC and MC40, respectively.

Neutron irradiation was performed using the TRIGA reactor of Jožef Stefan Institute (JSI), Ljubljana (Slovenia) [9]. Among the irradiated QA test pieces, test chips were tested at University of Toronto, while mini sensors were shared among JSI, Instituto de Física Corpuscular (IFIC, Spain) and University of Toronto.

Irradiation with  $\gamma$ -rays was performed using a cobalt-60 source at UJP PRAHA a.s. (Czech Republic) [10]. The QA testing was performed at the Academy of Science of the Czech Republic.

A fraction of the QA test pieces were sent to Instituto de Microelectrónica de Barcelona (IMB-CNM, Spain) for measurements of non-irradiated QA test pieces.



**Fig. 3.** Results from the charge collection efficiency measurement using mini sensors. (a) Collected charge as a function of the bias voltage. The red and blue dots correspond to results from proton-irradiated ( $1.6 \times 10^{15} n_{\text{eq}}/\text{cm}^2$ , CYRIC) and neutron-irradiated ( $1.6 \times 10^{15} n_{\text{eq}}/\text{cm}^2$ , TRIGA) mini sensors, respectively, while the black dots to results from a non-irradiated mini sensor. (b) Collected charge measured at the bias voltage of 500 V. The red solid (blue dashed) histogram show the distribution of the proton-irradiated (neutron-irradiated) mini sensors. The vertical line at  $6350\text{ e}^-$  shows the minimum required charge collection after  $1.6 \times 10^{15} n_{\text{eq}}/\text{cm}^2$  irradiation. All the mini sensors measured during the pre-production are shown in the histograms.

Target fluences were set at  $1.6 \times 10^{15} n_{\text{eq}}/\text{cm}^2$  for proton and neutron irradiations, and at 660 kGy for  $\gamma$ -ray irradiation at the maximum. Those were equivalent to the maximum expected values in the HL-LHC operation with  $4000\text{ fb}^{-1}$ , including a safety factor of 1.5. After irradiation, all QA test pieces were annealed for 80 mins. at  $60^\circ\text{C}$  before performing any testing, and the QA tests were performed at  $-20^\circ\text{C}$ . The QA threshold, based on which acceptance of the corresponding batch of the sensors is decided, for each measured parameter is determined to maintain a good signal-to-noise ratio for the tracker hits of the main sensor [4, 6, 11].

### 3. Results from quality assurance of the pre-production sensors

#### 3.1 Mini sensor

The charge collection efficiency was measured with  $\beta$ -rays from a strontium-90 source. A  $\beta$ -ray penetrating the mini sensor was detected by a trigger scintillation counter located below the mini sensor, and output charge was measured using the ALIBAVA system [12]. By fitting a Landau function convoluted with a Gaussian to the charge distribution, the charge collection efficiency was obtained from the peak of the Landau component. During the measurement, a bias voltage was applied to the backplane with keeping the bias ring to the ground. Details of the charge collection efficiency measurement are described in Ref. [13].

Figure 3(a) shows a few examples from mini sensors irradiated by protons and neutrons, as a function of the bias voltage. A conversion factor from the output values of the ALIBAVA to the number of electrons was obtained from measurements on non-irradiated sensors, assuming that the plateau of collected charge corresponds to 23,000 electrons, as done in Ref. [13]. The neutron-irradiated mini sensors show lower charge collection efficiency. This trend was observed in earlier studies [13]. The QA threshold was at  $6350\text{ e}^-$  at the bias voltage of 500 V in order to maintain sufficient signal detection efficiency. As seen in Fig. 3(b), all the mini sensors irradiated and measured during the pre-production were confirmed to have sufficient charge collection efficiency.

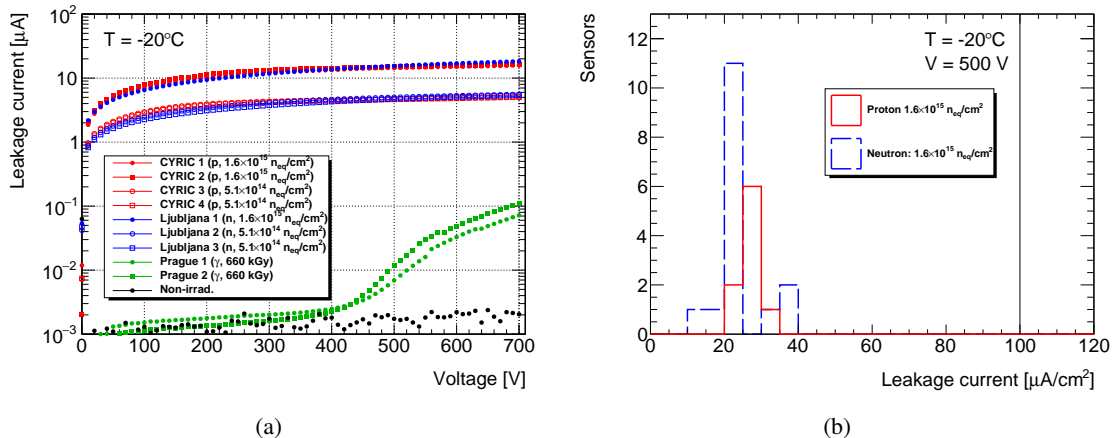


**Fig. 4.** Results from the  $I$ – $V$  measurements using MD8. (a) Examples of the  $I$ – $V$  characteristics for different types of irradiation. The red, blue and green dots correspond to the MD8 irradiated with neutron, proton and  $\gamma$ -rays, respectively, while the black dots show the results from a non-irradiated MD8. For the proton- and neutron-irradiated MD8, two different fluences are compared:  $1.6 \times 10^{15} n_{eq}/cm^2$  for the filled dots and  $5.1 \times 10^{14} n_{eq}/cm^2$  for the blank dots. For the  $\gamma$ -irradiated MD8, the dose was set at 660 kGy. (b) Distribution of the leakage current measured at the bias voltage of 500 V. The red solid (blue dashed) histogram corresponds to the proton- (neutron-)irradiated MD8. The vertical line at  $100 \mu A/cm^2$  shows the QA threshold. No result from the  $\gamma$ -irradiated MD8 is shown because increase of the leakage current is less significant.

### 3.2 MD8

An MD8 was used for the measurement of  $I$ – $V$  and  $C$ – $V$  characteristics, where  $I$ ,  $C$  and  $V$  denote the leakage current, the bulk capacitance and the bias voltage, respectively. During the measurement, a negative bias voltage was applied to the backplane while the bias ring was kept at the ground.

Results from the  $I$ – $V$  measurement are summarised in Fig. 4(a). As expected, the leakage current significantly increased after proton and neutron irradiations due to bulk damage, and the amount of leakage current was consistent for samples with the same fluence. The difference by a factor of three in the leakage current between  $5.1 \times 10^{14} n_{eq}/cm^2$  and  $1.6 \times 10^{15} n_{eq}/cm^2$  irradiations agreed well with the difference of the fluences. For the  $\gamma$ -irradiated MD8, the breakdown voltage tended to be lower. This was a known feature from the previous study [14]. It is noted that a high TID without bulk damages is not representative of the real experimental environment at HL-LHC.

The QA threshold for the MD8 measurements was the leakage current to be less than  $100 \mu A/cm^2$  with the bias voltage of 500 V. As shown in Fig. 4(b), all the measured MD8 satisfied the requirement. Additionally, the breakdown voltage needed to be above 500 V. Except the  $\gamma$ -irradiated MD8 which have the above-mentioned known feature, no breakdown was observed below 500 V.

### 3.3 Test chip

Using the test chip, six parameters discussed below were typically measured for the sensor QA; more results such as oxide properties are discussed in Ref. [6]. The results from the test chip measurements are summarised in Fig. 5.

**Bias resistance ( $R_{bias}$ ):** The test chip has several poly-silicon resistors to measure the bias resistance. In this measurement, a voltage sweep from  $-5$  V to  $+5$  V was applied to the poly-silicon, which has the exactly identical structure as the main sensor, and  $R_{bias}$  was calculated from the slope of the current as a function of the test voltage. Obtained  $R_{bias}$  are shown in Figure 5(a). The QA threshold for irradiated test chips was  $R_{bias}$  to be  $1.5 \pm 0.5$  MΩ at  $20^\circ C$ ; however, the measurement was performed at  $-20^\circ C$ . Since there was a known temperature dependence of

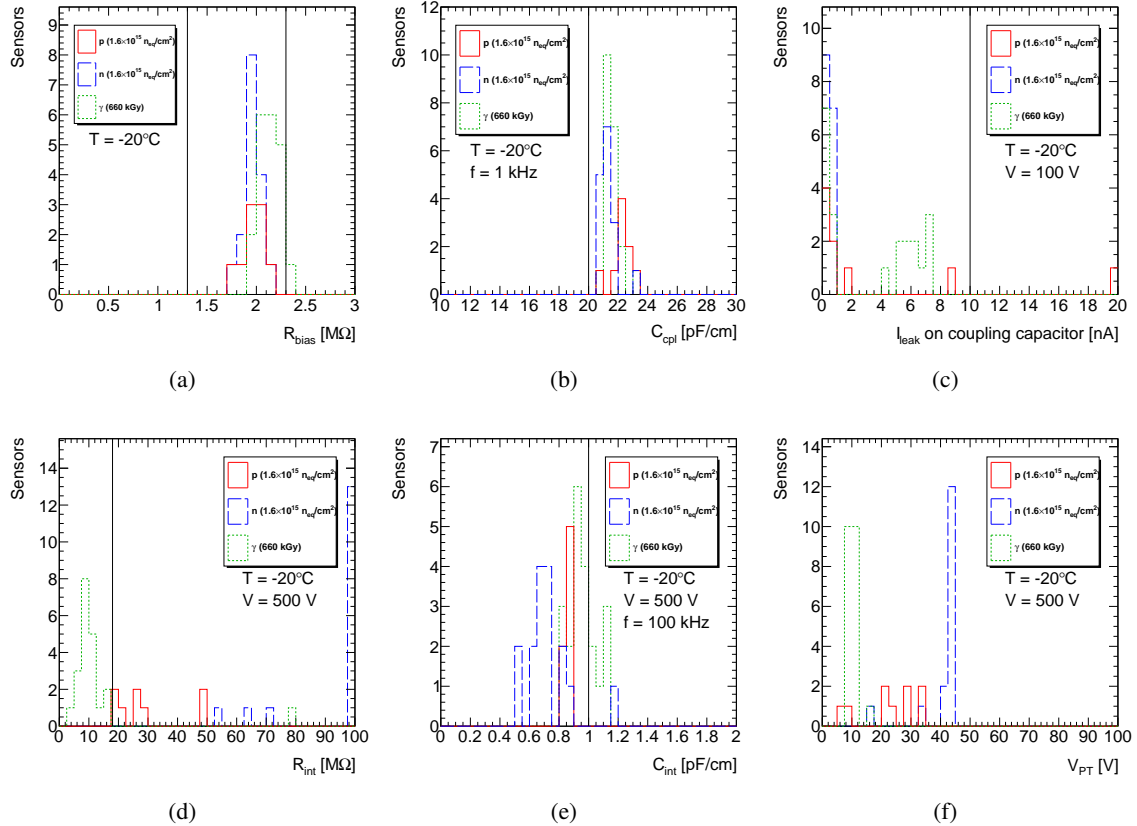


**Fig. 5.** Results from the test chip measurements: (a) bias resistance, (b) coupling capacitance, (c) leakage current on coupling capacitor, (d) interstrip resistance, (e) interstrip capacitance, and (f) punch-through protection voltage. All test chips irradiated to full fluence ( $1.6 \times 10^{15} n_{eq}/cm^2$  for proton or neutron irradiation; 660 kGy for  $\gamma$  irradiation) are shown in the histograms. In each plot, the QA thresholds are shown by the vertical lines.

$R_{bias}$  [15], the acceptance range at  $20^\circ\text{C}$  were extrapolated to  $-20^\circ\text{C}$ . This corresponds to about  $R_{bias} = 1.8 \pm 0.5 \text{ M}\Omega$ . While all the proton- and neutron-irradiated test chips showed  $R_{bias}$  within the acceptance range, test chips irradiated by  $\gamma$ -rays had a slightly larger  $R_{bias}$ , and there was one test chip outside the range. This was presumably due to a large oxide charge trapping in the vicinity of the poly-silicon resistor after ionisation damages. It is noted that pure  $\gamma$ -ray irradiation is not anticipated in the experimental environment of HL-LHC ATLAS. Besides, the slight increase of  $R_{bias}$  by  $\sim 10\%$  is not expected to influence the noise performance. Based on this study, the QA threshold for the  $\gamma$ -irradiated test chips was slightly increased by  $0.2 \text{ M}\Omega$ .

**Coupling capacitance ( $C_{cpl}$ ):** There is a square-shaped coupling capacitor, where an oxide layer is sandwiched between an aluminium electrode and an  $n^+$  implant. Its area,  $0.544 \text{ mm}^2$ , is equivalent to that of a 3.4-cm long strip. The capacitance was measured by applying a 1 kHz frequency, and the measured value was divided by the factor of 3.4 cm. For the sensor QA,  $C_{cpl}$  was required to be greater than  $20 \text{ pF/cm}$  after irradiation. As shown in Fig. 5(b),  $C_{cpl}$  was about  $22 \text{ pF/cm}$  on average with a small dispersion. All the test chips satisfied the requirement.

**Leakage current on the coupling capacitance:** The leakage current on the coupling capacitance was measured using the same structure as the  $C_{cpl}$  measurement, by applying up to  $100 \text{ V}$  on the oxide layer. The leakage current was required to be less than  $10 \text{ nA}$  at  $100 \text{ V}$  to ensure there is no pinhole. As shown in Fig. 5(c), all the test chips satisfied the requirement. One exception with

a large leakage current was understood due to mis-handling of the sensor, where a voltage far above 100 V was applied by accident, and therefore the oxide layer was broken. A low leakage current was confirmed with another test chip from the same batch.

**Interstrip resistance ( $R_{\text{int}}$ ):** There are three interdigitated strip structures, where two groups of strips are connected in parallel to each other, and the strips of each group are alternated with the strips of the other groups, maintaining the corresponding sensor strip pitch. The value of  $R_{\text{int}}$  was evaluated by measuring the  $I$ - $V$  characteristics between the two groups of strips. In this measurement, one of the interdigitated structures with 2.401-cm long strips was used. When applying the bias voltage of 500 V, test chips irradiated with protons or neutrons were required to have  $R_{\text{int}}$  at least 10 times greater than  $R_{\text{bias}}$ ; this corresponded to  $\gtrsim 18 \text{ M}\Omega$  at  $-20^\circ\text{C}$ . As shown in Fig. 5(d), all the proton- and neutron-irradiated test chips satisfied the requirement. However, the proton-irradiated test chips only marginally passed the QA threshold. This was attributed to the excessive TID; for example, in the  $1.6 \times 10^{15} \text{ n}_{\text{eq}}/\text{cm}^2$  irradiation at CYRIC, the test chips were expected to receive about 1.3 MGy, while 660 kGy was the nominal expected TID at HL-LHC. For the mass production, it was decided that the fluence of the proton irradiation was adjusted so that the TID corresponded to 660 kGy. The  $\gamma$ -irradiated test chips typically showed  $R_{\text{int}}$  lower than 15 M $\Omega$  due to effects from the large surface current. The results from the  $R_{\text{int}}$  measurement using the  $\gamma$ -irradiated test chips were not used for the sensor QA although the tests were performed to acquire a detailed understanding of the responses to the  $\gamma$ -ray irradiation.

**Interstrip capacitance ( $C_{\text{int}}$ ):** Using the interdigitated structure, the interstrip capacitance was measured using a 100 kHz frequency. The measured capacitance was normalised by the strip length of the interdigitated structure. After irradiation,  $C_{\text{int}}$  was required to be less than 1 pF/cm at the bias voltage of 500 V. As shown in Fig. 5(e), almost all the test chips satisfied the requirement; however, some test chips slightly exceeded the QA threshold. This was attributed to the design of the interdigitated structure; the additional stray capacitance can slightly increase the measured capacitance [6], also due to the parasitic capacitance in the test setup. It was therefore decided to accept these test chips.

**Punch-through voltage ( $V_{\text{PT}}$ ):** A punch-through protection structure is formed at the end of the strip implants in order to protect the AC coupling of strips from over-voltage [16]. If a large charge is collected on a strip implant, the voltage difference between the strip end and the bias ring becomes sufficiently high to allow the current to flow through the gap. The voltage which induces the punch through,  $V_{\text{PT}}$ , has to be sufficiently low to assure that the protection is activated in case of need, but well above 0 V in order not to cause a spontaneous breakdown. Since no specific value of  $V_{\text{PT}}$  is required in the sensor specifications, no threshold was defined during the sensor pre-production [17]. A measurement of  $V_{\text{PT}}$  was performed using a dedicated punch-through protection structure, where a test voltage between a strip and a bias ring was swept from 0 V until the punch through occurs. During the measurement, a negative bias voltage of 500 V was applied to the backplane while the bias ring was kept at the ground. The value of  $V_{\text{PT}}$  was defined at the voltage where the effective resistance between the strip and the bias ring became half of the bias resistance. As shown in Fig. 5(f), all the test chips had  $5 < V_{\text{PT}} < 50 \text{ V}$ , which was consistent with the results from the prototype sensors [18].

#### 4. Conclusion

In advance to the mass production of the strip sensors for the ATLAS ITk detector, the pre-production was carried out in the beginning of 2020, in order to confirm performance of the final version ATLAS18 strip sensors and to establish a solid and efficient workflow for the strip sensor QA. During the pre-production, 1101 wafers were produced, and 154 QA pieces were irradiated by protons (up to  $1.6 \times 10^{15} \text{ n}_{\text{eq}}/\text{cm}^2$ ), neutrons (up to  $1.6 \times 10^{15} \text{ n}_{\text{eq}}/\text{cm}^2$ ) or  $\gamma$ -rays (660 kGy).

In the pre-production QA, high quality of the ATLAS18 strip sensors was confirmed. Most of the QA pieces passed the test criteria, and a few pieces outside the acceptance range were understood to be due to test issues. They were solved before the mass production starts. Also, a few thresholds were slightly re-optimised based on the results from the pre-production QA.

Based on results and experiences from the pre-production, the mass production of the ATLAS18 strip sensor was approved, and started in July 2021, aiming to produce all of the 20,800 sensors by the beginning of 2025.

## Acknowledgement

This work was supported by the Canada Foundation for Innovation and the Natural Science and Engineering Research Council of Canada; the Ministry of Education, Youth and Sports of the Czech Republic coming from the projects LTT17018 Inter-Excellence and LM2018104 CERN-CZ; Charles University grant GAUK 942119; the Spanish R&D grant PID2021-126327OB-C22, funded by MCIN/ AEI/10.13039/501100011033 / FEDER, UE; JSPS Grant-in-Aid for Research Activity Start-up 20K22346; research core funding No. P1\_0135, funded by the Slovenian Research Agency.

The authors would like to thank the technical team at the UJP Praha a.s. (Czech Republic) for gamma irradiation of by cobalt-60 source; the TRIGA reactor at Jožef Stefan Institute (JSI) Ljubljana (Slovenia) for neutron irradiation; the University of Birmingham MC40 cyclotron (United Kingdom) for proton irradiation; the Cyclotron and Radioisotope Center (CYRIC) of Tohoku University (Japan) for proton irradiation.

## References

- [1] ATLAS Collaboration, CERN-LHCC-2017-021; ATLAS-TDR-030 (2017).
- [2] Latest ITk Pixel layout shown in ATLAS Collaboration, ATL-PHYS-PUB-2021-024 (2021).
- [3] ATLAS Collaboration, CERN-LHCC-2017-005; ATLAS-TDR-025 (2017).
- [4] Y. Unno et al., JINST **18**, T03008 (2023).
- [5] M. Ullán et al., Nucl. Instrum. Meth. A **981**, 164521 (2020).
- [6] P. Allport et al., JINST **17**, C11002 (2022).
- [7] Cyclotron and Radioisotope Center, Tohoku University, 6-3 Aoba, Aramaki, Aoba-ku, Sendai-shi, Miyagi 980-8578, Japan, <https://www.cyric.tohoku.ac.jp/en/>.
- [8] P. Dervan, R. French, P. Hodgson, H. Marin-Reyes and J. Wilson, Nucl. Instrum. Meth. A **730**, 101 (2013).
- [9] K. Ambrožič, G. Žerovnik and L. Snoj, Appl. Radiat. Isot. **130**, 140 (2017).
- [10] UPJ PRAHA a. s. Nad Kamínkou 1345, 156 10 Praha – Zbraslav, <https://ujp.cz/en/>.
- [11] I. Kopsalis et al., ATL-ITK-PROC-2022-017 (accepted by JINST).
- [12] R. M.-Hernandez, IEEE Trans. Nucl. Sci. **56**, 1642 (2009).
- [13] K. Hara et al., Nucl. Instrum. Meth. A **983**, 164422 (2020).
- [14] Y. Takahashi et al., Nucl. Instrum. Meth. A **699**, 107 (2013).
- [15] V. Latonova et al., Nucl. Instrum. Meth. A **1050**, 168119 (2023).
- [16] S. Mitsui et al., Nucl. Instrum. Meth. A **699**, 36 (2013).
- [17] From the results acquired through the sensor pre-production, ‘soft’ thresholds are defined for some of the technological parameters such as  $V_{PT}$ , and these have been made effective for the sensor mass-production. The purpose of the soft thresholds is to early detect possible deviations in the process. Although failure to the soft thresholds does not necessarily mean rejection of the corresponding sensors, it requires further detailed inspections on performance of the main sensors.
- [18] M. Mikestikova et al., Nucl. Instrum. Meth. A **983**, 164456 (2020).